LEGIBILITY NOTICE

A major purpose of the Technical Information Center is to provide the broadest dissemination possible of information contained in DOE's Research and Development Reports to business, industry, the academic community, and federal, state and local governments.

Although a small portion of this report is not reproducible, it is being made available to expedite the availability of information on the research discussed herein.

1

AUG 07 1985

LA-UR--85-2460

DE85 015710

CONF-850706--28

TITLE DETONATION REACTION ZONE STUDIES ON TATB EXPLOSIVES

AUTHOR(S) W. L. Seitz
H. L. Stacy
Jerry Wackerle

SUBMITTED TO The Eighth Symposium (International) on Detonation

DISCLAIMER

Los Alamos National Laboratory
Los Alamos, New Mexico 87545

DETONATION REACTION ZONE STUDIES ON TATB EXPLOSIVES

W. L. Seitz, H. L. Stacy, and Jerry Wackerle
Los Alamos National Laboratory
Los Alamos, NM 87545

Interface velocity histories between heterogeneous detonating explosives and transparent windows, separated by a thin (13 µm) aluminum shim, have been obtained with an image-intensified rotating-mirror streak camera and a Fabry-Perot velocity interferometer system. Seven TATB-based explosives were studied with PMMA windows for typically three charge lengths. Two of the explosives were also studied with LiF windows. In each case a non-steady detonation was observed, with each increasing charge length showing a corresponding increase in the interface velocity histories. Time resolution and velocity error are estimated to be about 6 ns and 2% respectively. Numerical simulations for one of the explosives, for which a shock-strength modified Arrhenius rate law (DAGMAR) and an assumed equation of state (HOM) had been previously calibrated with shock initiation gauge data, gave good agreement with the experimental velocity histories.

INTRODUCTION

The detonation reaction zone in heterogeneous explosives has been the subject of many research studies. Numerous experimental techniques such as the plate-push [1], electromagnetic gauge [2], rate stick [3], Fabry-Perot interferometer [4], and wide-angle Michelson interferometer [5] have been used in an attempt to obtain CJ detonation pressures, detonation reaction zone thicknesses, spike pressures, and other details of the detonation process. In spite of the considerable research on the subject many unanswered questions concerning the flow in the reaction zone remain.

We describe in this paper an experimental study of the detonation reaction zones of seven TATB-based explosives by measuring the interface velocity histories between the detonating explosives and transparent windows, separated by a thin (13µm) aluminum shim, with a Fabry-Perot velocimeter system. The seven explosives were a fine and coarse lot of PBX 9502 (95/5 weight percent TATB/Kel-F), PBX 9503 (80/15/5 weight percent TATB/HMX/Kel-F), X-0407 (70/25/5 weight percent TATB/PETN/Kel-F), and three particle-size distributions of 1.8 g/cm³ (7% porous) TATB (so called standard grind, superfine, and micronized).

Numerical simulations of the interface velocity histories for the 1.8 g/cm³ superfine TATB using a shock-strength modified Arrhenius reaction rate law (DAGMAR) and an assumed equation of state (HOM) that had been previously calibrated to Manganin-gauge data [6] are also presented and found to be in good agreement with experiment.

EXPERIMENTAL

An image-intensified rotating-mirror streak camera and a Fabry-Perot velocity interferometer system [7] were used to measure interface velocity histories between detonating explosive samples and transparent windows. A 13-µm aluminum shim was placed between the explosive and window to provide a reflective surface. Experiments were performed with PMMA windows for typically three charge lengths of 13, 25, and 50 mm for seven explosives. LiF windows were used for experiments on the fine lot of PBX 9502 and 1.8 g/cm³ superfine TATB with charge lengths of 13 and 25 mm. All experiments were driven with a P-40 plane-wave lens, 25 mm of Composition B, and 10 mm of 6061 aluminum as shown in Fig. 1. This driving system was chosen to give a relatively prompt initiation of detonation (less than 2 mm of run for each of the seven explosives, without having an overdriven detonation. Planarity of the

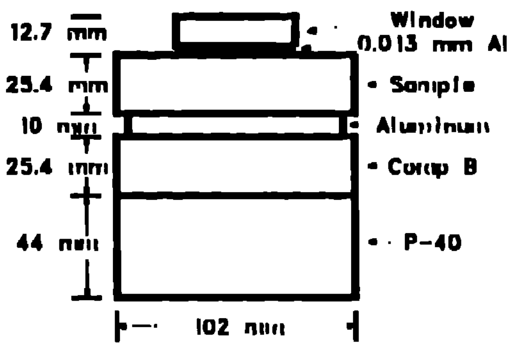

Fig. 1. Typical configuration for explosive driver and target system.

initiating wave was about 40 ns. A diameter/length ratio of 2 or greater was used to avoid edge effects. Experiments were carefully constructed to hold necessary tolerances. Initial temperatures were controlled at 20 ± 1°C. All PMMA windows were constructed from Rohm and Haas type II UVA Plexiglas with a density of 1.186 ± 0.001 g/cm³. The LiF windows were X-cut single crystals.

A schematic of the Fabry-Perot interferometer system [8,9] is shown in Fig. 2. The laser was a 12-watt (all lines) Spectra-Physics Model 171-07 argon-ion, which was operated single frequency at 514.5 nm with an output power of about 3 watts. The laser beam was sent to the target and the reflected light from the target (which had been carefully prepared to produce diffuse reflections) was collimated with lens L1 and directed to the Fabry-Perot interferometer. A cylindrical lens L2 positioned just before the interferometer converged the beam in one direction. Fringes produced by the Fabry-Perot were focused onto the camera slit with lens L3. By using a cylindrical lens to converge the beam in only one direction, constructive interference fringes appear as dot pairs at the camera slit, rather than the usual rings produced by a Fabry-Perot. Considerable intensity gain is attained by using the cylindrical lens. Typically the focal length of lens L2 was chosen to produce about 4 fringe pairs.

A Burleigh Model RC-110 Fabry-Perot interferometer with 50.8-mm-diameter mirrors was used. The mirrors were flat to within λ/200 with reflectivities of 93%.

Figure 3 shows the image-intensified rotating-mirror streak camera (I²RMC). A 40-mm-diameter International Telephone and Telegraph image-intensifier tube [10] and a high aperture lens (f/2.5) were mounted such that the image formed at the streak-camera film plane was projected onto the image-intensifier tube. A magnification of 1.36 was used between the streak-camera film plane and the image-intensifier tube. The writing speed at the intensifier tube was about 21 mm/μs.

A Doppler shift in wavelength of the reflected laser light resulting from target motion, beginning at shock arrival time, produces a corresponding shift in fringe spacing. For our choice of window materials, target interface velocities are related to fringe spacing by [7]

$$V = \frac{c\lambda}{4t(1+k)} \cdot \left| \frac{d'^2_{n,m} - d^2_n}{d^2_{n+1} - d^2_n} - m \right| , \quad (1)$$

where c is the velocity of light in vacuum, λ is the initial wavelength of the laser, t is the Fabry-Perot mirror spacing, (1+k) is the correction factor for the change in index of refraction for the window material, d_n and d_{n+1} are the distances between dot pairs for the n and n+1 static fringes, and $d'_{n,m}$ is the dynamic fringe spacing for the nth fringe. The number of fringes shifted, m, at shock arrival time must be determined from some previous knowledge of the target velocity or nominally identical experiments must be performed with different fringe constants (cλ/4t). In the present work cλ/4t was 3.6 mm/μs/fringe and the target velocities were known to within one fringe constant.

A typical streak record of fringes is shown in Fig. 4. Streak records were digitized with an optical comparator, and position data were transformed into velocities and times with equation (1) and the known camera writing speed. Estimated time resolution and velocity errors were 6 ns and 2 %, respectively. As would be expected, the reverberations in the 13-μm aluminum shim, estimated to be about 5 ns, were not resolved. All times are referenced to shock arrival at the window. Data points were typically read such that velocities were obtained at 5-ns intervals for the first 50 ns

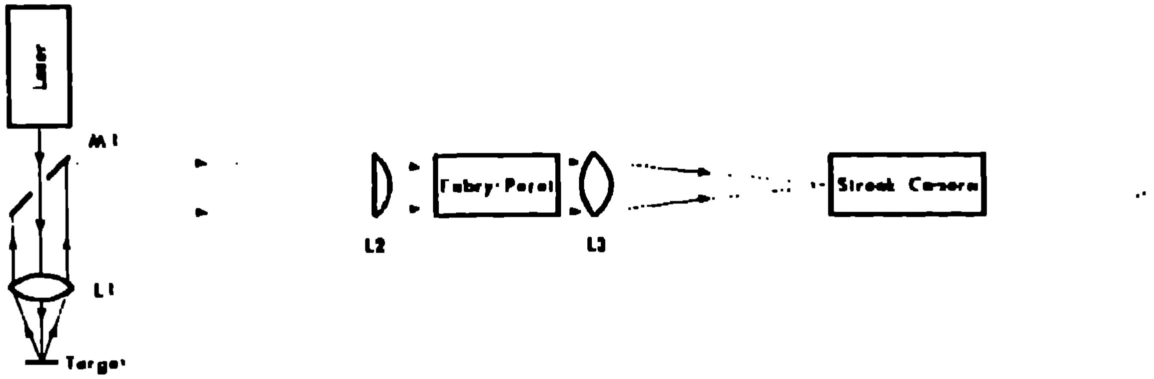

Fig. 2. Schematic of the Fabry-Perot interferometer system.

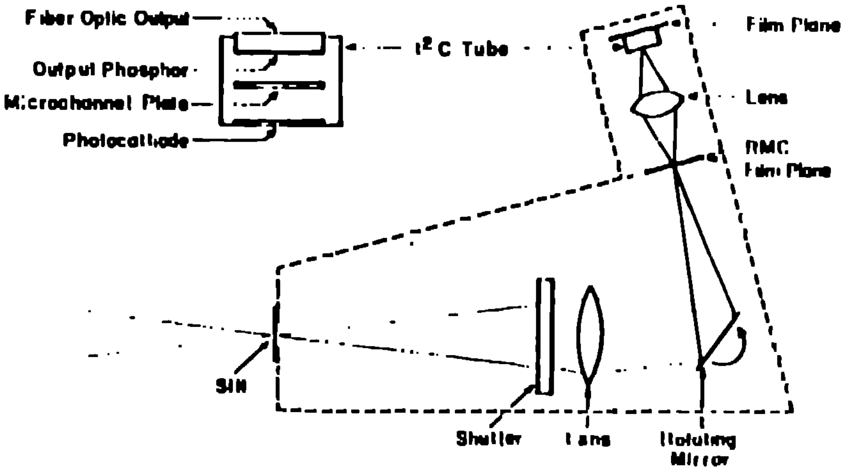

Fig. 3. Schematic of rotating mirror streak camera (I²RMC).

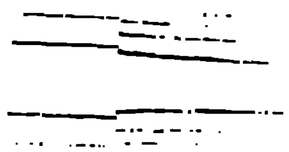

Fig. 4. Typical streak record with a total streak time of 1.8 μs.

and at 20-ns intervals for the remainder of the record.

RESULTS

Figure 5 shows typical scatter and a functional fit to the data for the fine PBX 9502. The purely empirical functional form,

$$V = ae^{-bt} - ct + d, \qquad (2)$$

was found to give a good fit to the velocity histories. Due to a strong correlation between constants and the different data ranges for each experiment, comparisons between specific constants for the various explosives are not meaningful. For times greater than the coverage of the data, the fit predicts arbitrarily large negative or positive velocities; therefore, extrapolation outside the data range should be avoided.

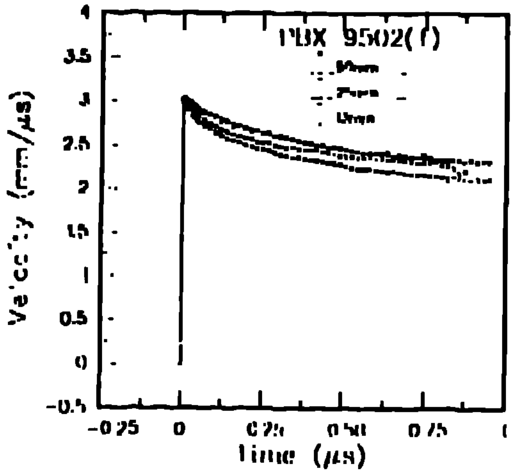

Fig. 5. Comparison of functional form with actual data for fine PBX 9502 with PMMA window.

Functional fits to the experimental data points for the seven explosives studied are shown in Fig. 6. A tabulation of explosive densities and functional fit constants for PMMA and LiF windows are given in Tables 1 and 2, respectively. All of the interface velocity histories have the common feature that one cannot discern an outstanding demarcation that might be associated with attaining a Chapman-Jouguet state. This condition for TATB-based explosives and others, was also noted in Refs. [2] and [5]. An additional common feature of the seven explosives studied is the increase in interface velocity histories with increasing run distances. As discussed in Ref. [2], this is indicative of a failure to attain a steady detonation in the run distances of the experiments.

SOME CALCULATIONAL RESULTS

As a first step in examining the data, we have calculated impedance-match solutions for the interface velocities using the classical Zeldovich-von Neumann-Doering (ZND) model of a steady detonation, and equation-of-state representations of the unreacted Hugoniot and fully reacted products in common use at Los Alamos. A typical result is displayed in pressure-particle velocity space in Fig. 7. Here the right-hand solid curve is the unreacted Hugoniot for the explosive, the left-hand solid curve is the products isentrope through the Chapman-Jouguet (CJ) state, and the dashed line connects this state with the von Neumann (VN) spike condition along the Rayleigh line of slope $\rho_0 D$ (where ρ_0 is the initial density and D is the detonation velocity). The unreacted Hugoniots are cast in the common linear shock velocity-particle velocity form U = C + Su. The constants C and S were obtained for all the explosives by least-square fitting to initial U-u data obtained from explosives wedge experiments; these data are obtained mostly at states well below the CJ condition, and typically have considerable scatter. The CJ isentrope is calculated with a Becker-Kistiakowsky-Wilson (BKW) equation of state [11]. These calculations are generally well-calibrated to measured detonation velocities and Hugoniot data.

The upper, dotted curve of Fig. 7 is the calculation of the reflected-shock Hugoniot and rarefaction isentrope for the unreacted explosive, determined using a Mie-Grüneisen equation of state. The conditions of continuity of pressure and particle velocity at a contact surface provide a prediction of the initial interface particle velocities at the intercept of the dotted curve with the Hugoniot curves for LiF (chain dotted) and PMMA (chain dashed). In the context of the ZND model, the calculation is a legitimate test of the extrapolation of our unreacted Hugoniots.

The "extended impedance match solution" shown by the lower dotted curve is less legitimate. The locus is a reflection of the CJ isentrope, and may considerably oversimplify the match of the CJ state condition into a window.

The interface velocities calculated by impedance-match solution are listed in Table 1, along with the more important characterization constants. Single listings are given for PBX 9502 and 1.8-g/cm³ TATB because we have been unable to discriminate differences in Hugoniot data for different particle sizes of these two compositions. In Fig. 6 the calculated interface velocities are indicated by arrows for matching into the VN and CJ states. The VN points are reasonably consistent with observation.

We have conducted a few preliminary computational simulations of the observed reaction zones with our modification of the PAD 1D numerical hydrocode [12]. Fickett has previously shown that such numerical calculations introduce spurious small amplitude oscillations in a nominally steady reaction zone profile [13]. We eventually achieved reasonably

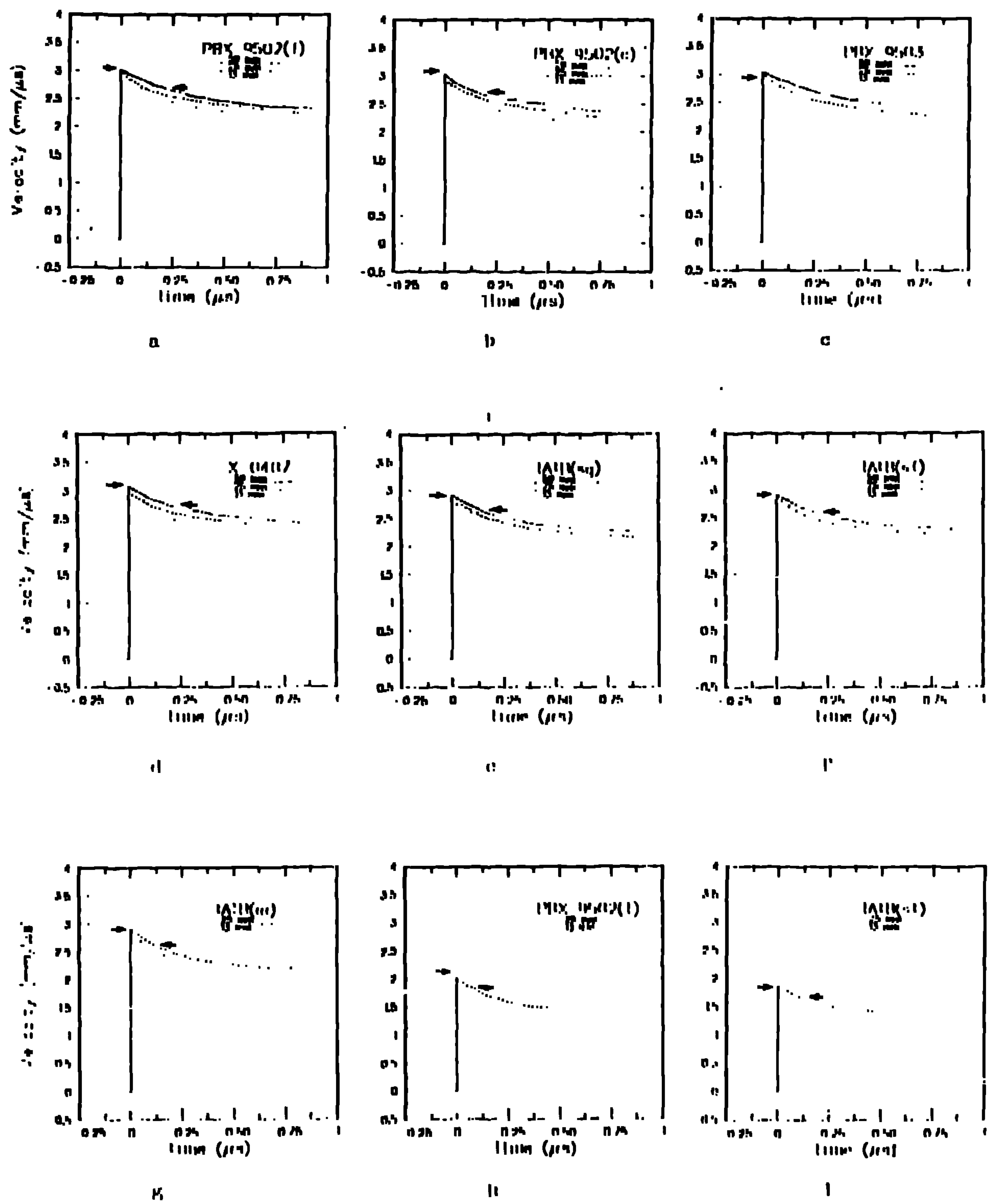

Fig. 6. Functional fit of $V = ae^{-bt} - ct + d$ to measured interface velocity histories for fine PBX 9502(a), coarse PBX 9502(b), PBX 9503(c), X-0407(d), 1.8 g/cm³ standard grind TATB(e), 1.8 g/cm³ superfine TATB(f), and 1.8 g/cm³ micronized TATB(g) with PMMA windows, and fine PBX 9502(h) and 1.8 g/cm³ superfine TATB(i) with LiF windows. Arrows show calculated VN spike and CJ interface velocities.

TABLE 1
Initial density and constants for the empirical fit, $V = ae^{-bt} - ct + d$, for the explosive configurations with PMMA windows.

Explosive Material	Charge Length (mm)	Initial Density (g/cm³)	a (mm/μs)	b (μs⁻¹)	c (mm/μs²)	d (mm/μs)
PBX 9502(f)	13	1.893	0.51474	5.76843	0.31886	2.39794
"	25	1.893	0.39464	9.57291	0.41747	2.59944
"	50	1.891	0.76128	2.65347	-0.00616	2.24753
PBX 9502(c)	13	1.895	0.44476	9.85036	0.48507	2.50223
"	25	1.890	0.28930	9.87736	0.53415	2.67900
"	50	1.892	0.27690	12.69448	0.51769	2.74842
PBX 9503	13	1.876	0.48589	11.82438	0.42754	2.46726
"	25	1.872	0.47241	6.49196	0.33891	2.53148
"	50	1.878	2.49192	1.12038	-1.08401	0.54019
X-0407	13	1.859	0.50022	6.58338	0.32477	2.42810
"	25	1.858	0.36162	7.89929	0.39056	2.61543
"	50	1.855	0.39526	6.12678	0.33013	2.67922
Superfine	13	1.800	0.52690	6.00780	0.24853	2.29458
"	25	1.804	0.52713	6.23868	0.18610	2.34638
"	50	1.780	0.53345	4.64913	0.12170	2.38598
Std. Grind	13	1.805	0.57074	4.26505	0.17297	2.23027
"	25	1.807	0.54894	5.11110	0.17268	2.31207
"	50	1.799	0.56060	4.39603	0.11041	2.35296
Micronized	13	1.810	0.56821	6.02492	0.26353	2.26314
"	25	1.803	0.66430	4.49368	0.08306	2.23083

TABLE 2
Initial density and parameters for configurations with LiF windows.

Explosive Material	Charge Length (mm)	Initial Density (g/cm³)	a (mm/μs)	b (μs⁻¹)	c (mm/μs²)	d (mm/μs)
PBX 9502	13	1.893	1.16244	2.85397	-0.67360	0.79127
"	25	1.892	1.15112	2.79590	-0.67165	0.85717
Superfine	13	1.796	0.82673	2.38543	-0.21712	0.94906
"	25	1.801	0.64970	3.99618	-0.23873	1.21643

smooth results using about 20 cells/mm, a linear combination of linear (Landshoff) and quadratic (Richtmeyer-von Neumann) artificial viscosity, and on the suggestion of Charles Forest, the imposition of 25% of the compressive artificial viscosity on rarefaction. Although these artifices were less than satisfying, they were found to give PAD calculations of steady detonation reaction zones in reasonable agreement with exact calculations of reaction-zone state histories as they evolve along the Rayleigh line. We found that we could simulate the standard driving system described earlier using 31 mm of Composition B with the "hot start" option of PAD, which constructs a CJ detonation at the explosive-alloy interface and imposes an analytic formulation of the Taylor wave. This configuration was used to drive the calculations of the experiments.

In this paper, we report only our most successful simulations, for 1.8 g/cm³ superfine TATB, for which we had previously used embedded-gauge data to develop an empirical reaction-rate correlation [6]. This correlation was

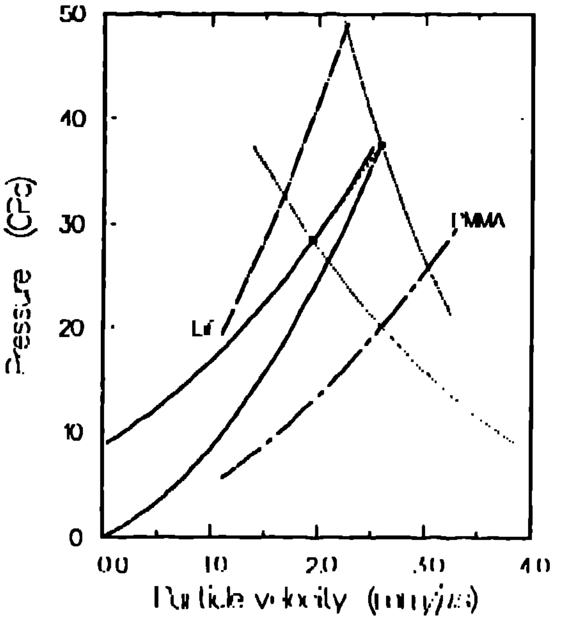

Fig. 7. Impedance-match solutions for interface velocities.

developed using the HOM equation of state [11], which assumes the unreacted explosive and products state equations described earlier, ideal mixing of specific volume and internal energy of the two constituents, and that the two phases are in pressure and temperature equilibrium. We used both a Newton's iteration algorithm [14] and a computer subroutine devised by Charles Forest for the numerical calculations.

The rate correlation calibrated in [6] was the "Direct Analysis Generated Modified Arrhenius Rate," or DAGMAR, first found useful for representing PBX 9404 [15]. It is formulated,

$$r = \frac{\partial \lambda}{\partial t} = Z_0(1 - \lambda)\, p_s^n\, e^{-T^*/T}, \quad (3)$$

where λ is the mass fraction reacted, p_s the pressure of the first shock at a given mass point, T the current temperature (calculated in the HOM equation of state) and Z_0, n and T^* constants. The same HOM and DAGMAR constants (Z_0 = 0.0158, n = 2.61, T^* = 1861 K, pressure in GPa) as employed in the previous work [6] were used in the simulations. Simulations with these constants indicated a 21-GPa input shock and approximately a 1-mm run distance to detonation, which is consistent with that observed for 1.8-g/cm³ TATB [6]. The detonation incident on the window was thus fully initiated and self-supporting for all thicknesses of TATB.

The numerical simulations of interface velocities were performed for 13- and 25-mm thicknesses of TATB, for both PMMA and LiF windows. The results are compared with data and the empirical fitting functions in Fig. 8. The numerical calculations neglected the aluminum foil, and the plotted values are from the first computational cell in the windows. Reaction histories calculated in the last cell of the explosive are shown as dashed lines in Fig. 8, and serve better to identify the calculated reaction zone durations. Agreement of computed and observed particle velocities during this reaction time is generally good; disagreement at later times could be the result of our failure to properly represent the driver system or the products equation of state, or both. Some test calculations showed that the velocity histories were not extremely sensitive to the choice of rate constants; however, calculations with Z_0 multiplied or divided by 3/2 were in discernibly poorer agreement than those shown.

DISCUSSION

The resolution of our Fabry-Perot laser velocimeter appears to be adequate to resolve the relatively wide reaction zone in TATB-based explosives. As was concluded in a previous study on one of these explosives (PBX 9502) with a better time resolution [5], detonation waves in all the explosives we studied appear to have a ZND character. Sharply rising, unreactive shocks are followed by decreasing particle velocities, pressures, densities, and internal energies through the reaction zones. This view is in good agreement in nearly every case with the impedance-match solutions for the VN spike state; where agreement is not as good, the imprecision of the existing Hugoniot data will admit to adjustment.

The experimental profiles for the seven explosives are rather similar in character, reflecting the fact that the interface velocity measurements are not highly sensitive to modest changes in reaction rates. This was also noted in the numerical simulations. Subtle, unknown differences in reaction rate magnitudes and form, generally associated with particle-size distributions, are much more manifest in high-pressure

TABLE 3
Explosive Constants and Interface Velocities

Explosive	ρ_o (g/cm³)	C (mm/μs)	S	u_{CJ} (mm/μs)	D (mm/μs)	PMMA VN (mm/μs)	PMMA CJ (mm/μs)	LiF VN (mm/μs)	LiF CJ (mm/μs)
PBX 9502	1.890	2.400	2.050	1.953	7.695	3.1	2.6	2.2	1.7
PBX 9503	1.875	2.400	2.200	NA	7.840	2.9	NA	2.2	NA
X-0407	1.866	3.000	1.800	2.002	7.773	3.1	2.7	2.3	1.7
Pure TATB	1.800	2.054	2.357	1.984	7.552	2.9	2.6	1.8	1.6

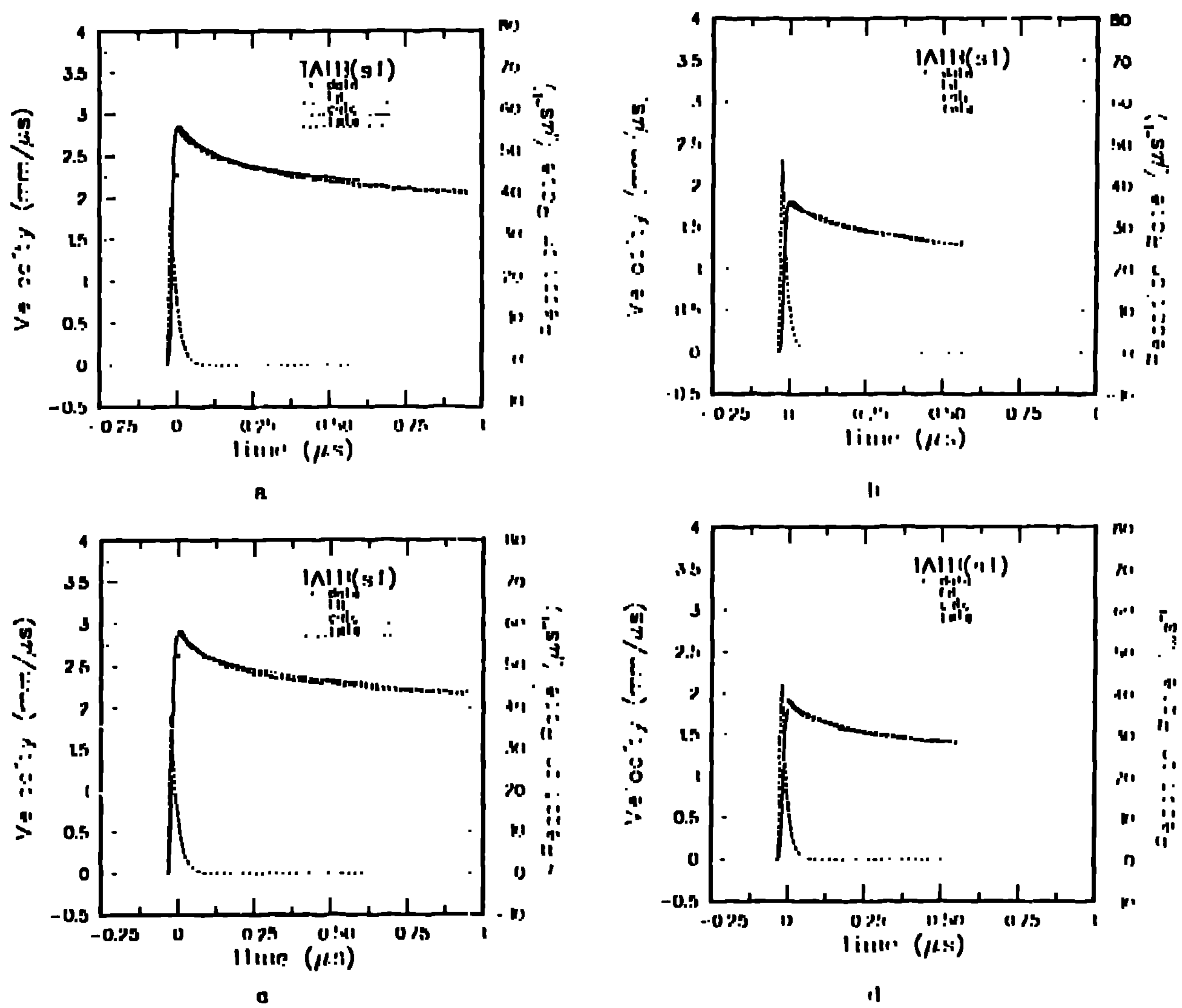

Fig. 8. Comparison of numerical simulations (solid curve) with both data (symbols) and the empirical fitting function (chain dotted) for 13-mm run with PMMA (a), 13-mm run with LiF (b), 25-mm run with PMMA (c), and 25-mm run with LiF (d). Calculated reaction rate histories are also shown for each case with a dashed curve.

short-shock experiments [16] and detonation wave-spreading observations [17].

With sufficient modification of the FAD numerical hydrocode, we were able to simulate, reasonably well, the velocity histories for 1.8-g/cm³ superfine TATB (the one TATB-based explosive for which we have a reaction rate calibration). The previous correlation was used without modification, despite being calibrated at pressures less than half those encountered with the detonation incident on a LiF window. In fitting the individual velocity histories at different run distances numerical calculations succeeded in simulating the non-steady character of the detonation.

In part, the successful simulation actually may result from the properties of the DAGMAR form. In particular, this rate correlation combines multiplicative factors in depletion, shock strength, and current state. Such a form has been repeatedly demonstrated to be effective in simulating a variety of shock initiation problems, and is beginning to be characteristic of more physically-based rate forms, such as Krakatoa [18] and the explicit hotspot model of Johnson, Tang, and Forest [14].

In simulating detonations colliding with inert windows, DAGMAR sets the p_s factor with the nearly constant VN spike pressure before the collision, and thus differs from a simple-depletion rate only in the modification due to the temperature dependence. With our HOM representation for 1.8-g/cm^3 TATB, the 2050 K VN spike temperature increases about 12% through a detonation reaction zone, increases 15% with the shock reflected from a LiF window, and decreases 10% with the rarefaction from PMMA. These conditions lead to little difference in the shape of the rate histories for PMMA and LiF windows seen in Fig. 8, with the higher initial rate value from the higher impedance-match temperature for the LiF windows being the most prominent feature. The reaction rate histories for each of the calculated cases have about the same 150-ns duration. With the impedance-match solutions indicating a 37-GPa initial pressure for the LiF window and a 22-GPa initial pressure for the PMMA window, one would not expect to obtain so small a difference in rates and in scaled interface velocity histories with a rate form strongly dependent on current pressure.

The DAGMAR and HOM representations also have properties leading to numerical simulations without a distinct CJ point in the velocity profile and an increasing interface velocity with run distance, as are consistently observed. Bdzil and Davis have made a detailed theoretical study of unsteady, underdriven detonation [19]. They considered an explosive which is driven by a two-step heat-release rate. About 90% of the energy release is fast; the remainder is slow. Their analysis shows that the release of the last 10% of the energy is what controls the transients that precede the establishment of steady detonation. The physical basis for their results can be traced to a simple property of ZND detonation; the tangency of the Rayleigh line and totally reacted Hugoniot curve. Because of the tangency condition, the final 10% of the energy release controls about 50% of the pressure profile in the reaction zone. In addition, the flow is sonic at the point of tangency. As a consequence, the energy released near the end of the reaction zone is transported towards the shock very slowly. The result is an unsteady detonation wave for run distances of many tens of reaction zone thicknesses, with a building up of the velocity histories much as we observe and simulate numerically. In our case, the DAGMAR first-order depletion factor approaches full reaction asymptotically. In detonating 1.3-g/cm^3 TATB, HOM indicates that over 80% of the reaction occurs in less than 50% of the state change from the VN to the CJ state, characteristic of most solid explosives. Our numerical simulation of unsteady detonations is thus a natural consequence of the properties of our rate and equation-of-state form and the general characteristics of an almost ZND detonation.

The velocity profiles observed in the other six explosives are all similar to those for 1.8-g/cm^3 superfine TATB. They could probably be simulated with a rate form having a peak value of a few tens of reciprocal microseconds, a first-order depletion factor, and very little other dependence on current state. To extend the rate to treating initiation problems the rate should have, like DAGMAR, more current-state dependence as pressures are reduced.

ACKNOWLEDGEMENTS

We greatly appreciate the technical assistance of F. J. Dilharri, O. D. Harkleroad, and S. K. Salazar. We also thank J. B. Bdzil and C. A. Forest for valuable discussions.

REFERENCES

1. Russell E. Duff and Edwin Houston, "Measurement of the Chapman-Jouguet Pressure and Reaction Zone Length in a Detonating High Explosive," J. Chem. Phys. 23, p. 1268, 1955.

2. W. C. Davis, "Magnetic Probe Measurement of Particle Velocity Profiles," Sixth Symposium on Detonation, Office of Naval Research Report ACR-221, p. 637, 1976.

3. A. W. Campbell and Ray Engelke, "The Diameter Effect in High-Density Heterogeneous Explosives," Ibid., p. 642, 1976.

4. L. M. Erickson, H. G. Palmer, N. L. Parker, and H. C. Vantine, "Free-Surface Velocity Measurements of Plates Driven by Reacting and Detonating RX-03-BB and PBX-9404," Proceedings of the American Physical Society Topical Conference, Menlo Park, California, p.553, 1981.

5. S. A. Sheffield, D. D. Bloomquist, and C. M. Tarver, "Subnanosecond Measurements of Detonation Fronts in Solid High Explosives," J. Chem. Phys. 80, p. 3831, 1984.

6. Allan B. Anderson, M. J. Ginsberg, W. L. Seitz, and Jerry Wackerle, "Shock Initiation of Porous TATB," Seventh Symposium on Detonation, Office of Naval Research Report NSWC MP82-334, p. 385, 1981.

7. W. L. Seitz and H. L. Stacy, "Fabry-Perot Interferometry Using An Image-Intensified Rotating-Mirror Streak Camera," Proc. SPIE on High Speed Photography, Videography, and Photonics, 427, p. 186, 1983.

8. M. Durand, P. Leharrague, P. Lalle, A. Le Bihan, J. Morrian, and H. Pujols, "Interferometric Laser Technique for Accurate Velocity Measurement in Shock Wave Physics," Rev. Sci. Instru. 48, p. 275, 1977.

9. D. R. Goosman, "Measuring Velocities by Laser Doppler Interferometry," Energy and Technology Review, Lawrence Livermore National Laboratory Report UCRL-52000-79-3, 1979.

10. J. H. Parker, Ray Engelke, W. Morton, and A. S. Lundy, "Resolution Loss in Microchannel Plate Image-Intensifier Tubes at High Gains," SPIE Semin. Proc., 190, LASL Optics Conf., 1979.

11. Charles L. Mader, "Numerical Modeling of Detonation," University of California Press, Berkeley, 1979.

12. W. Fickett, "PAD, A One-Dimensional Lagrangian Hydrocode," Los Alamos Scientific Laboratory Report LA-5910-MS, 1975.

13. W. Fickett, "Accuracy of the Conventional Lagrangian Scheme for One-Dimensional Hydrodynamics," Los Alamos Scientific Laboratory Report LA-6454, 1976.

14. J. Johnson, P. Tang, and C. Forest, "Shock-Wave Initiation of Heterogeneous Reactive Solids," J. Appl. Phys. 57, p. 4323, 1985.

15. Jerry Wackerle, R. L. Rabie, M. J. Ginsberg, and A. B. Anderson, "A Shock Initiation Study of PBX 9404," Proceedings of the Symposium on High Dynamic Pressures, Paris, France, p. 127, 1978.

16. W. L. Seitz, "Short-Duration Shock Initiation of Triaminotrinitrobenzene (TATB)," Proceedings of the American Physical Society Topical Conference, Santa Fe, New Mexico, p. 531, 1983.

17. C. A. Honodel, J. R. Humphrey, R. C. Weingart, R. S. Lee, and P. Kramer, "Shock Initiation of TATB Formulations," Seventh Symposium on Detonation, Office of Naval Research Report NSWC MP 82-334, p. 425, 1981.

18. J. Vanpoperynghe, J. Sorel, H. C. Pujols, "Experiments and Numerical Simulation of High Explosive Delayed and Lowed Detonation," This Symposium, 1985.

19. J. B. Bdzil and W. C. Davis, "Time-Dependent Detonations," Los Alamos Scientific Laboratory Report LA-5926-MS, 1975.